Influence of vacancy diffusional anisotropy: Understanding the growth of zirconium alloys under irradiation and their microstructure evolution

Benjamin Christiaen, Christophe Domain, Ludovic Thuinet, Antoine Ambard, A. Legris

Influence of Vacancy Diffusional Anisotropy: Understanding the growth of zirconium alloys under irradiation and their microstructure evolution

B. Christiaen[a,b,c], C. Domain[a,c], L. Thuinet[b,c], A. Ambard[a,c], A. Legris[b,c]

[a]EDF-R&D, Département Matériaux et Mécanique des Composants (MMC), Les Renardières, F-77818 Moret sur Loing Cedex, France
[b]Univ. Lille, CNRS, INRAE, Centrale Lille, UMR 8207 - UMET - Unité Matériaux et Transformations, F-59000 Lille, France
[c]Laboratoire commun EDF-CNRS Etude et Modélisation des Microstructures pour le Vieillissement des Matériaux (EM2VM), France

Abstract

In this work, we propose a series of Object Kinetic Monte Carlo simulations complemented by an analytical model that allows rationalizing a certain number of experimental facts related to the growth of high purity, recrystallized zirconium alloys under irradiation. Our vision of the phenomenon rests essentially on vacancy diffusion anisotropy (with faster diffusion in the basal planes than perpendicular to them) that is necessary to lead to the formation of layers of <a> prismatic interstitial dislocation loops parallel to the basal plane. The acceleration of the deformation under irradiation and this localization of the damage are strongly connected. An analytical model developed using the concepts of difference of anisotropic diffusion between vacancies and interstitials makes it possible to account for the observed phenomena.

Introduction

Neutron irradiation in crystalline materials produces displacement cascades that generate great amounts of point defects (vacancies and interstitials) near the point of impact. Some picoseconds after the collision it remains cascade debris consisting of point defects (single-vacancies and single-interstitials) and of cluster of point defects. These defects diffuse, agglomerate and / or emit point defects to produce large defects such as dislocation loops or cavities. It is the growth of defect clusters that leads to an evolution of the microstructure and which are at the origin of the macroscopic growth of recrystallized zirconium alloys under irradiation in non-corrosive environment. This growth can be divided into 3 distinct phases referred as stages I to III in the following. Stage I is characterized by a rapid increase in free growth for neutron doses around 1×10^{25} n.m^{-2}. During stage II, a stationary regime is established. Finally, stage III also called "breakaway" corresponds to an acceleration of free growth generally observed for high neutron doses of the order of 3-7 $\times$ 10^{25} n.m^{-2}. These stages are correlated with microstructural features thoroughly described in the review by Griffiths [1]. Measuring the alloys dimension changes due to irradiation and performing detailed transmission electron microscopy analyses on irradiated samples allowed to conclude that:

i-in low-dose irradiated zirconium alloys the point defects gather as dislocation loops with a Burgers vector $\langle a \rangle = \frac{1}{3}\langle 1\,1\,\bar{2}\,0\rangle$ called " <a> or prismatic loop" with the habit planes of the loop parallel or close to the prismatic $\{1\,0\,\bar{1}\,0\}$ planes of the hcp structure. Such loops are readily produced during irradiation. The nature of the loops (interstitial or vacancy), their density and diameter depend on several parameters such as the irradiation temperature, grain size or the presence of alloying elements (see [2], [3], [4] for instance). An important point is that these loops are mostly aligned in rows or layers parallel with the trace of the basal plane (0001). These loops were the first to be observed in irradiated Zr alloys.

ii-The <c> loops began to be observed for high irradiation doses, typically greater than 3.0-7.0 × 10^{25} n.m^{-2} with a primary knock-atom (PKA) of energy E>1 MeV. These loops are mainly localized in the basal plane with a Burgers vector $\frac{1}{6}\langle 2\ 0\ \bar{2}\ 3\rangle$ (although some loops with a Burgers vector [0001] have also been observed) which has a component parallel to the $\vec{c}$ axis. Contrary to <a> loops, they are only vacancy in nature. They have been observed at temperatures between 560-773 K and range in size from 0.1 to about 1.0 μm diameter depending on the temperature. In many cases, they are concomitant with an increased irradiation growth rate, a phenomenon known as irradiation breakaway that, depending on alloy composition and microstructure and on irradiation conditions, is observed after an incubation period or dose of about 3.0-7.0×10^{25} n.m^{-2} (E>1 MeV). For these reasons, the breakaway is intimately associated to the appearance of the <c> loops. Recent works have confirmed that no <c> loop smaller than 10 nm could be identified [5] in irradiated Zr alloys using TEM whereas its resolution readily allows it which is in qualitative agreement with the work of Griffith [1]. This suggests that other mechanisms than progressive growth by accumulation of individual vacancies might be at work to explain the sudden appearance of these objects.

An appealing explanation of the main observed phenomena (i-ii) has been proposed by the so-called Diffusional Anisotropy Difference (DAD) model [6] that is based on the difference of anisotropic diffusion of interstitials and vacancies. The DAD model assumes that interstitials diffuse faster in the basal plane than along the $\vec{c}$ axis and this more markedly than vacancies whose diffusion is supposed to be isotropic. This hypothesis naturally leads to interstitials being captured by prismatic loops. For evident geometrical reasons their capture cross section is high for objects moving preferentially in the basal plane and low for those moving parallel to $\vec{c}$. For similar reasons, <c> loops will capture vacancies preferentially. Therefore, the

DAD model proposes a kinetic-topological view that allows explaining the growth of interstitial <a> loops and of vacancy <c> loops but gives no simple explanation of the observed localization of the <a> loops. Recently, the hypothesis put forward by Woo in the 1980s concerning diffusion anisotropy has been strongly questioned and even invalidated by the calculation of the diffusion coefficients of point defects by ab initio atomic simulation in Zr [7] [8] [9]. These recent results indicate that self-interstitials diffuse slightly faster in the basal plane than along $\vec{c}$ but also reveal that vacancies exhibit the same behavior with a greater anisotropic ratio. In addition, a recent work gives indirect experimental evidence that self-interstitial atoms diffusion anisotropy in Zr is much lower than initially thought and supposed by the DAD [2]**.** Despite this strong questioning, the DAD model is still popular within the scientific community probably because of its simplicity and its explanatory capacity. Furthermore one cannot exclude that it might be operational in the case of alloys containing small amounts of Fe for instance, for which an extrinsic mechanism of diffusion may work to explain the observed [10] Zr faster self-diffusion in the basal plane than parallel to $\vec{c}$. Other models have been proposed and among them the BEK [11] and the Production Bias Model (PBM, [12]) assume that the numbers of mobile vacancies and self-interstitials produced by the cascade are not equal. It is less clear however how these models can explain the results obtained with electron irradiation which are qualitatively the same that under neutron irradiation.

The objective of this work is to propose an explanation of the recrystallized zirconium alloys growth and of their microstructure evolution under irradiation. To this end, Object Kinetic Monte Carlo (OKMC) calculations were performed in order to describe the microstructure evolution under neutron irradiation of a pure Zr crystal with no additional elements. The parameters of the OKMC were obtained from experimental data when available or from

atomic scale calculations using DFT based ab initio energy models and/or empirical potentials. The results of the simulations, which agree with the most salient experimental features, are explained in the framework of a revisited Diffusional Anisotropy Difference model that is based on the same approach that the original DAD model but assumes in high purity alloys a larger diffusional anisotropy for vacancies than for interstitials in agreement with the most recent atomic scale calculations and experimental evidence as explained before. The following of the work is divided in three parts: first the OKMC model and its parameterization are described, the main technical aspects being detailed in the Supplementary Material section, then the results are presented and interpreted in the framework of a revisited DAD model followed by a discussion and conclusion sections.

Description of the OKMC model

A general description of the OKMC method can be found in [13]. The model considers the time evolution of a population of defects characterized by a jump frequency ν_M. Objects can move in an underlying spatial grid that mimics the atomic lattice, although the atoms in regular lattice positions are not explicitly taken into account (see Supplementary Material section). Objects can react between them (annihilation, aggregation, creation) with a frequency ν_R attached to each possible reaction. On the whole a resident time algorithm is used to determine the time evolution of the population of defects. The less defects in the simulation box the more efficient the modeling is. Details of the simulation are given in the Supplementary Material section.

The main parameters used to perform the calculation in this work are summarized in Table 1. For simplicity objects of size $n > 1$ are considered immobile which constitutes a strong assumption that will be discussed.

Table 1 : General parameters of the OKMC used in this work

Parameter		Vacancy	Interstitial
$\nu_{1,\perp}^{a}$ (s^{-1})		5.62×10^{13} [8]	3.35×10^{11} [14]
$\nu_{1,\parallel}^{a}$ (s^{-1})		7.82×10^{13} [8]	7.49×10^{11} [14]
$\nu_{n}^{emis}(s^{-1})$	Cavity	$\nu_{n}^{emis} = \nu_{1,\perp} \times n^{2/3}$	
	Disl. Loop	$\nu_{n}^{emis} = \nu_{1,\perp} \times n^{1/2}$	
$E_{1,\parallel}^{m}$(eV)		0.66 [8]	0.26 [8]
$E_{1,\perp}^{m}$(eV)		0.55 [8]	0.23 [8]
E_{n}^{emis}		$E_{n}^{emis} = E_{n}^{b} + E_{1,\perp}^{mig}$	
E_{n}^{b}		$E_{n}^{b} = E_{f}(n=1) - (E_{f}(n) - E_{f}(n-1))$	
R	Cavity, pyramid	$\left(\frac{n.3.V_{at}}{4\pi}\right)^{\frac{1}{3}} Z_{i,v}$	
	‹a› loop	$\left(\frac{n.ac}{2\pi}\right)^{\frac{1}{2}} Z_{i,v}$	
	‹c› loop	$\left(\frac{n.a^2\sqrt{3}}{4\pi}\right)^{\frac{1}{2}} Z_{i,v}$	
Z_v, Z_i		1 [15]	1.1 [15]
r_{iv}(Å)		$5Z_v$	$5Z_i$

The following defects are modeled in our OKMC runs:

i- Point defects (vacancies and self-interstitials), small interstitial clusters with planar geometry as well as cavities are taken into account when the defects aggregates have a low size (less than 20 point defects). Their stability has been previously established [16], [17].

ii-When cavities and planar interstitial defects grow and reach the threshold of 20 point defects, their morphology evolves to become:

1-Interstitial <a> loops (from the evolution of planar interstitial defects): there are three different variants <a1>, <a2>, <a3> corresponding to the three equivalent directions in the basal plane. In the absence of an applied stress they are produced with equal probability. The same procedure is used to generate equivalent <a> vacancy loops.

2-Vacancy <a> loops or stacking fault pyramids (SFP) result from the evolution of the cavities. The transition from the cavity to an <a> loop (respectively SFP) occurs with a probability p (respectively 1-p), a parameter whose influence will be studied. As for interstitial <a> loops, in the absence of an applied stress, the three different equivalent crystallographic variants <a1>, <a2>, <a3> are produced with the same probability. The switch from cavities to SFP has been established from stability criteria explained in [16]. The fact that cavities can also become vacancy <a> loops is suggested by the presence of <a> vacancy loops in irradiated materials ([2]).

iii- Vacancy loops with a <c> component (Burgers vector $\frac{1}{6}\langle 2\ 0\ \bar{2}\ 3\rangle$ and 1/2 [0001]) have been simulated. According to [16] we assume that <c> loops are formed by the collapse of SFPs when they reach a size of 400 vacancies. It should also be mentioned that SFP were previously observed at the heart of some cascades during the molecular dynamic runs used to generate the primary damage for our OKMC simulations (as noticed in [18]). They are similar in nature to the stacking fault tetrahedrons commonly observed in irradiated FCC alloys but until now they have not been experimentally detected in Zr alloys. Schematics of the evolution of these defects with their size is drawn in Figure 1. The largest objects are loops.

In Table 1, $\nu^{a}_{1,\perp}$ (s^{-1}) and $\nu^{a}_{1,\parallel}$ (s^{-1}) are the attempt jump frequencies in the basal plane and parallel to $\vec{c}$ for point defects [8], [14]. The values for interstitials were estimated from the D_0 values given in [14] (obtained using molecular dynamics with an empirical potential) and assuming a jump distance of 3.23 Å whatever the jump. Together with the migration energies $E^{m}_{1,\parallel}$ and $E^{m}_{1,\perp}$ given in [8] and that compare well with the values in [7] and [9] , they combine to give the vacancy and interstitial diffusion anisotropy ratio (respectively noted VDAR and IDAR in the following). Using the data of Table 1 we obtain at 600 K $D^{\perp}/D^{\parallel}$=6.0 and 1.2 respectively for vacancies and interstitials values that compare well with those in [7] (5 and 3 respectively) and in [9] (2.6 and 1.9 respectively). The influence of this ratio on the OKMC results has been studied and is presented in this work. The experimental data concerning vacancy anisotropy of diffusion in Zr and in Zr alloys is scarce and available only at temperatures close to the α–β transition temperature 1137 K. In [19] and [10] the self-diffusion in high purity Zr single-crystals was measured in thermal equilibrium conditions. In this case, the anisotropy of tracer diffusion is directly related to vacancy anisotropy diffusion (vacancy mechanism of diffusion). In [19] the VDAR varies between 1.2 and 2.3 for 936 K<T<1099K (non monotonic behavior), while in [10] a VDAR= 1.9 at 1110 K is given. If one takes a value of VDAR around 2 at 1000 K and an Arrhenius law for both $D^{\perp}$and $D^{\parallel}$, assuming that the anisotropy is due to the sole migration enthalpy leads to a VDAR close to 10 at 600 K, which is the order of magnitude of the values used in this work (between 4 and 6). As mentioned previously, there is also indirect experimental evidence that the self-interstitial atoms anisotropy is much lower [2] than initially assumed by the DAD model.

The pre-exponential coefficient ν_n^{emis} represents the product of the coefficient $\nu_{1,\perp} = \nu^{a}_{1,\perp} \exp\left(\frac{E^{m}_{1,\perp}}{kT}\right)$ and the number of sites n_s on the surface of the object containing n point

defects. n_s depends on the shape of the object under consideration. For cavities, n_s is defined as the ratio between the surface of a sphere of size n and the area of a sphere of size 1. In the same way n_s for the loop is defined as the ratio between the surface of a torus of size n and that of a torus of size 1.

The emission energy is the sum of the binding energy and migration energy.

The binding energies were determined from the fitting of atomic scale data described in detail in [16] for the large size objects. For small size ones they were calculated using the DFT code VASP and are described in [17]. Additional information is given in the Supplementary Material section.

In order to account for long-range elastic interactions, bias has been introduced for all objects. To this end, we consider a capture efficiency (Z_i) larger for interstitials than for vacancies (Z_v). The values in Table 1 were estimated from [15] and [20]. Typical values of 1.1 and 1 respectively for interstitials and vacancies were adopted. Numerically the capture efficiency was used as a multiplying factor for the capture radius (R in Table 1) for each type of sink, which leads to an absorption bias by the sinks of the order of 0.1 in favor of the interstitials. The expressions for R in Table 1 are described in the Supplementary Material section.

A typical recombination radius of 5 (respectively 5.5) Å was taken for vacancies (repectively interstitials).

Results

Two parameterizations have been developed: a "reference" parameterization based on the most recent data from our atomic scale calculations and simulation results from the literature (reported in Table 1), and an "optimized" parameterization with some parameters adjusted to experimental results. Meanwhile, in order to validate the point defect diffusivity data reported in Table 1, we performed isochronal annealing simulations.

Isochronal annealing

We test the parameters of the model by means of isochronal annealing simulations. The generated data were compared with experimental data from different irradiation conditions (neutron, electron) at a very low temperature of the order of 4K. In order to activate the mobility of the defects, the material is annealed progressively by isochronous increments while measuring its resistivity. In this way, it is possible to follow indirectly the density of the defects present in the material. In the simulation, we have randomly introduced 4000 Frenkel pairs (uncorrelated vacancy-interstitial pairs) in the simulation box (containing 200 × 200 × 200 orthorhombic cells) in order to reproduce in a simplified way the primary damage generated by electron irradiation corresponding to 1.25×10^{-4}dpa. To simulate the annealing, the temperature increases of 5 K every 1000 seconds. When the mobility of vacancies and self-interstitials is activated, they begin to annihilate, reducing the number of defects present in the simulation box. As soon as there is no more defects in the material, it is completely annealed. Diffusion data of vacancies and self-interstitials are detailed in Table 1. Figure2 compares the simulation of an isochronal annealing with electron and neutron irradiation experiments. The results show a reasonable agreement with the experiments with an activation of the migration of self-interstitials and vacancies that occurs respectively at 100 K

and 250 K, the closest agreement being obtained with electron irradiation results from Dworschak et al [21]. The differences between experiments and modeling can be mainly due to the lack of spatial correlation between vacancies and self-interstitials in our model and to the absence of mobility of small point defect clusters in the simulation.

Reference simulations

We obtained the results of the simulations presented in this section with the so-called "reference" parameterization. It is built using the defects previously described, a primary damage introduced in the form of 50 keV cascade debris from an available database containing approximately 300 simulations (source term used for the production of defects) as well as values from the literature and presented in Table 1. It must be emphasized that no ad hoc adjustment has been made. The size of the simulation box is set at 300 × 195 × 195 orthorhombic cells (see Supplementary Material Fig SM2), which corresponds to dimensions close to 100 × 100 × 100 nm^3. We present five simulations in this section. In three of them, the migration anisotropy of the vacancy is taken into account, while for the last two, the migration of the vacancy is considered as isotropic. For the anisotropic simulations, different values of p were used: p = 0, 0.5 and 1.0. Isotropic simulations are performed with the probabilities p = 0 and p = 0.5. Table 2 summarizes the simulation parameters used for the results presented in this section.

First, anisotropic diffusion simulations are presented.

The size distribution (Figure 3), the free growth (Figure 4) as well as the microstructure (Figure 5) are analyzed and discussed.

At 1 dpa, when p = 0, <c> loops are present in very low density (1×10^{17} m^{-3}) with an average diameter of about 30 nm. The low density of loops can be explained by the relatively high emission capacity of the pyramids, the vacancies are then redistributed in the system. The pyramids are also present in low density ($2\text{-}3 \times 10^{19}$ m^{-3}) for an average diameter of 2 nm. Interstitial <a> loops are present with higher density than pyramids and <c> loops. Extrapolating the results of [2] at 1 dpa, we obtain a density number too high by about two orders of magnitude and an average size an order of magnitude below, a difference that will be analyzed. Contrary to vacancy objects, interstitial objects have very low emission rate. This allows them to form stable nuclei more easily. What limits their growth is essentially the interstitial-vacancy recombination rate that increases with the density of vacancies in the system.

The vacancy emission rate of pyramids and cavities is larger than the one of <a> vacancy loops. Then, when <a> vacancy loops are present (p > 0), the density of <a> interstitial loops is greater.

At p = 0.5, the size distribution of <a> vacancy loops and pyramids is very different, although they are formed from cavities with the same probability. The pyramid density is larger than that of <a> vacancy loops (up to 12 times) while their size is smaller (up to 40 times). At the investigated irradiation dose, no pyramid has reached the threshold size to switch to <c> vacancy loops, which are therefore absent in the simulation box.

The knowledge of the distribution of defects and the determination for each of them of their stress-free strain or eigenstrain allows determining the global deformation as a function of irradiation dose (see Supplementary Material section).

Table 2: Parameters used for the simulations. Only the migration anisotropy of vacancies has been adjusted for the isotropic simulations with respect to the parameters of Table 1.

Simulation conditions	Anisotropic	Isotropic
T (K)	600	600
Flux (dpa.s^{-1})	1×10^{-6}	1×10^{-6}
Domain size (nm^3)	100×100×100	100×100×100
PKA energy (keV)	50	50
p	0 ; 0.5 ; 1	0 ; 0.5
$E^m_{v,\parallel}$(eV)	0.66	0.6
$E^m_{v,\perp}$(eV)	0.55	0.6
$\nu_{1,\parallel}$(s^{-1})	7.82×10^{13}	6.72×10^{13}
$\nu_{1,\perp}$(s^{-1})	5.62×10^{13}	6.72×10^{13}

Figure 4 shows the mean basal and <c> deformations, $\frac{\bar{\varepsilon}_{xx}+\bar{\varepsilon}_{yy}}{2}$ and $\bar{\varepsilon}_{zz}$, as a function of the dose, these values being expressed in the basis (x//$[\bar{1}2\bar{1}0]$, y//$[\bar{1}010]$, z//$[0001]$). When <a> vacancy loops are considered (p = 0.5 and p = 1), there is a slight growth in the z direction and a significant contraction in the x and y directions, which is in complete disagreement with experiments. Eigenstrains of <a> loops show that the calculated contraction induced by <a> vacancy loops is stronger than the expansion induced by <a> interstitial loops (Supplementary Material Section) in such extent that even a low density of <a> vacancy loops is sufficient to generate a contraction along the x and y directions. The fact that <a> vacancy loops induce a contraction in the basal plane higher than the expansion of the <a> interstitial loops is due to the fact that according to our atomic scale simulations the latter have an habit plane close to $\{1\ 0\ \bar{1}\ 0\}$ in agreement with experiments while the former have a $\{1\ 1\ \bar{2}\ 0\}$ habit plane which overestimates their eigenstrain. Positive deformation in the z direction results from the slightly positive eigenstrains of <a> interstitial and vacancy loops along $\vec{c}$ and the absence of <c>vacancy loops.

Conversely, when <a> vacancy loops are not considered (p = 0), growth along the x and y axes, and contraction in the z direction are observed. In particular, there is an acceleration of

these phenomena around 0.8 dpa. The microstructural analysis depicted Figure 5 shows that this acceleration coincides with to two facts that are correlated:

i-the growth of <c> vacancy loops and

ii-the formation of a banding of <a> interstitial loops along the basal plane.

Beyond a critical size, pyramids transform into <c> vacancy loops with a lower emission capacity, and as a result, the interstitial <a> loops can then grow faster, both effects contribute to the acceleration of growth.

The stacking of <a> interstitial loops is a microstructural feature that has been reported many times but seldom explained. We show that its formation is due to the diffusion anisotropy of the point defects and more precisely to the fact that vacancies diffuse faster in the basal plane than perpendicularly to it. Indeed, two supplementary simulations were carried out, assigning isotropic diffusion to the vacancies. Figure 6 and Figure 7 respectively show the microstructure at 1dpa and the free growth for simulations performed with p = 0 and p = 0.5: in these cases there is no stacking of <a> interstitial loops in the microstructure and no acceleration growth. Like for anisotropic simulations, when one considers <a> vacancy loops (p = 0.5), $(\bar{\varepsilon}_{xx} + \bar{\varepsilon}_{yy})/2$ is negative and $\bar{\varepsilon}_{zz}$ is positive, which is qualitatively similar to the results obtained with anisotropic diffusion, and in disagreement with the experiments.

Therefore, the simulations most in agreement with the experimental results of macroscopic growth are those for which <a> vacancy loops are not considered (p = 0). In the case of anisotropic diffusion, there is an acceleration of the free growth around 0.8 dpa. This dose value is relatively low compared to experiments, which measures a transition for doses

between 3 and 7 dpa. It has been found that this acceleration is accompanied by the rapid growth of the <c> vacancy loops and an increase in their density, but also by the formation of a stacking of small interstitial<a> loops in the basal plane. It has also been noticed that the interstitial loops present in these stackings grow faster (those located outside them undergo very low growth rate). Moreover, this formation seems to occur concomitantly with the increase of the density of the pyramids. When this density increases, the probability of recombination between a vacancy and a self-interstitial object decreases, which leads to promote the growth of interstitial loops.

When <a> vacancy loops are considered (p> 0), they are rather numerous and very large due to their low emission. The deformation calculations obtained by considering these objects show that there is a growth along the <c> axis and a significant contraction in the <a> directions in disagreement with experiments. As mentioned, this situation may be originated by an overestimation of the eigenstrain generated by the <a> vacancy loops. For this reason, we have chosen to disregard this object in the following optimized simulations, delaying a more detailed analysis of their influence for future works.

In the case of isotropic simulations, even if the sign of the growth can be that observed experimentally (for p = 0) there is no growth acceleration. Moreover, no stacking of interstitial loops was observed either for p = 0 or for p = 0.5.

We can therefore partially conclude that the formation of the alignment of <a> interstitial loops in the basal plane is due to the anisotropic diffusion of the vacancies and that as soon as these stackings are formed in the microstructure, there is a growth acceleration. Recent experimental results [3] [4] clearly showed a correlation between <a> loops banding in the basal plane and growth of <c> vacancy loops and will be further discussed.

The goal of the next section is to present an analytical diffusion model to explain the formation of this specific stacking in the basal plane when anisotropic diffusion is taken into account.

Analytical diffusion model

This part aims at showing that the specific location of the interstitial prismatic loops in rows or layers parallel with the trace of the basal plane (0001) is the most favorable one for their growth. To this end and to start with, we will suppose for simplicity that the dislocation loops are aligned along the axis of a cylinder (see Figure 8). The quantities of vacancies and self-interstitials absorbed by the stacking can then be calculated as a function of the orientation of the cylinder. For this purpose, the stacking is assimilated to an equivalent point defects absorbing cylinder of axis **l** and the crystal basis is **R0** = ($[\bar{1}2\bar{1}0]$,$[\bar{1}010]$,$[0001]$). Two cases are specifically studied :(a) **l** stays in the prismatic plane containing one of the 3 equivalent dense directions <a> (for example $[\bar{1}2\bar{1}0]$ in Figure 8a) and (b) **l** stays in the basal plane (Figure 8b). In both cases, the stacking orientation is defined by the angle θ between **l** and <a>.

The diffusion equation for each point defect is solved in a new basis (x', y', z') such that **l//z'**. This new basis is obtained from **R0** by a rotation of an angle θ around direction $[\bar{1}010]$ in case (a) and by two successive rotations respectively of 90° around $[\bar{1}010]$ and θ around direction $[0001]$. In the new basis (x', y', z'), the equation of the equivalent absorbing cylinder is:

$$\left(\frac{x'}{R_{x'}}\right)^2 + \left(\frac{y'}{R_{y'}}\right)^2 = 1$$

In case (a), $R_{x'} = R\cos\theta, R_{y'} = R$ whereas in case (b), $R_{x'} = R,\ R_{y'} = R\cos\theta$. We then follow the same procedure as in [22]. The anisotropic diffusion equation in this basis is given by:

$$\left(D_{x'}\frac{\partial^2}{\partial x'^2} + D_{y'}\frac{\partial^2}{\partial y'^2}\right)C = 0$$

Where C is the point defect concentration. In case (a):

$$D_{x'} = \sin^2\theta D_{\perp} + \cos^2\theta D_{||}$$

$$D_{y'} = D_{\perp}$$

In case (b):

$$D_{x'} = D_{||}$$

$$D_{y'} = D_{\perp}$$

Where $D_{\perp}$ and $D_{||}$ are respectively the diffusion coefficients perpendicular and parallel to the basal plane.

We then make the following variable transformation:

$$x'' = \left(\frac{\overline{D}}{D_{x'}}\right)^{\frac{1}{2}} x'$$

$$y'' = \left(\frac{\overline{D}}{D_{y'}}\right)^{\frac{1}{2}} y'$$

The diffusion equation expressed by means of these new space variables becomes:

$$\overline{D}\left(\frac{\partial^2}{\partial x''^2} + \frac{\partial^2}{\partial y''^2}\right)C = 0$$

At this stage, the diffusion equation above is valid whatever the value of $\overline{D}$, a proper value for this parameter will be chosen hereafter. The boundary conditions in (x'',y'',z'') are C = 0 on the absorbing cylinder defined by the following equation:

$$\frac{x''^2}{(\overline{D}/D_{x'}^{eff})R^2} + \frac{y''^2}{(\overline{D}/D_{y'}^{eff})R^2} = 1$$

We assume that point defects come from a reservoir maintained at a constant concentration $\overline{C}$, and located at a distance R_∞ away from the center of the equivalent absorbing cylinder, then $C = \overline{C}$ on the elliptic cylinder defined by:

$$\frac{x''^2}{(\overline{D}/D_{x'}^{eff})R_\infty^2} + \frac{y''^2}{(\overline{D}/D_{y'}^{eff})R_\infty^2} = 1$$

In case (a):

$$D_{x'}^{eff} = \tan^2\theta D_\perp + D_{||}$$

$$D_{y'}^{eff} = D_\perp$$

In case (b):

$$D_{x'}^{eff} = D_{||}$$

$$D_{y'}^{eff} = D_\perp$$

Like in [22], the current I per unit length of the equivalent cylinder can be deduced:

$$I = \overline{D}\overline{C}\frac{2\pi}{\eta_{R_\infty} - \eta_R}$$

With

$$\overline{D} = \left(D_{x'}^{eff} D_{y'}^{eff}\right)^{1/2}$$

$$\eta_R = \frac{1}{2}\ln\left(\frac{\sqrt{D_{y'}^{eff}} + \sqrt{D_{y'}^{eff}}}{\left|\sqrt{D_{x'}^{eff}} - \sqrt{D_{y'}^{eff}}\right|}\right)$$

$$\square = \left(\overline{D}/\min(D_{y'}^{eff}, D_{x'}^{eff})\right)^{1/2} R/\cosh\eta_R$$

$$\eta_{R_\infty} = \ln\left(\frac{2R_\infty}{\square}\sqrt{\frac{2\,\bar{D}}{D_{x'}^{eff} + D_{y'}^{eff}}}\right)$$

By noting respectively I_I and I_V the currents of self-interstitials and vacancies, the favored stacking direction of <a> interstitial loops is the one maximizing I_I/I_V. By using the diffusion coefficients of Table SM1 and [14], we obtain the curves reproduced in Figure 9. In each case (a) and (b), the maximum value of I_I/I_V is reached for $\theta = 0$: spatial arrangement of the loops which favors the maximum net flux of self-interstitials corresponds to a stacking along the direction parallel to the Burgers vector. Note however that the effect of the orientation of the cylinder within the basal plane is almost immaterial, the observed decrease for $\theta = 90°$ is due to the fact that by construction at this angle the cylinder becomes a ribbon since the axis of the cylinder lies in the habit plane of the loop.

Therefore, this simple model shows that alignments in the basal plane are preferred to alignments outside it. Moreover, inside the basal plane all the alignment directions are equally probable, which implies a random distribution of loops inside the basal plane. This has been recently confirmed by TEM observations [23] and is in agreement with the results obtained in OKMC simulations when anisotropic diffusion of the vacancies is taken into account.

The next section of this chapter proposes to study the effect of the vacancy diffusion anisotropy on growth acceleration.

Optimized simulation

The "optimized" parameterization has been adjusted to reproduce the available experimental data. In the previous sections, different parameters have been identified as significant in the

irradiation growth mechanism, namely the magnitude of vacancy diffusion anisotropy and the frequency of emission of the pyramids. More precisely, it has been shown that this anisotropy plays a role in the macroscopic growth acceleration and that the stability of the pyramids influence the size and density of the interstitial objects and <c> loops. To adjust the vacancy diffusion anisotropy and the stability of the pyramids, the vacancy migration energy parallel to the <c> axis $E_{v,\parallel}^{m}$ and the emission energy of the pyramids $E_{n,pyra}^{emis}$ are modified.

The experimental data used to adjust our results are provided in [2] and [24]. Using microscopy analysis of ion-irradiated zirconium samples, the authors were able to obtain information on the evolution of density and average size of <a> interstitial loops [2] and <c> vacancy loops [24] depending on the irradiation dose. Their results, presented in Table 3, show that the experimental average size of the objects is much higher than the one obtained in our simulations, but also that their density is smaller. However, knowing the average size and the density of the objects, these data can be converted in density of point defects. This quantity is used to adjust our parameters.

Table 3: Experimental data for ‹a› and ‹c› loops.

	Dose (dpa)	Average diameter $\bar{d}$ (nm)	Object density (m^{-3})	Point defect density (m^{-3})
‹a› interstitial loops [2]	0.45	32	6.4×10^{20}	6.25×10^{24}
‹c› vacancy loops (Zr4 ion) [24]	2.9	21	1.44×10^{20}	1.10×10^{24}
	4.1	22	2.84×10^{20}	2.39×10^{24}
	7.0	24	3.86×10^{20}	3.87×10^{24}

‹c› vacancy loops (M5 ion) [24]	4.1	20	1.71×10^{20}	1.19×10^{24}
	7.0	23	2.72×10^{20}	2.50×10^{24}

Table 4 gathers the parameters that have been modified from the reference parameterization. $E_{v,\parallel}^{m}$ is slightly changed, from 0.66 to 0.64 which implies a noticeable modification of the vacancy anisotropy ratio from 6.0 to 4.1. An amount of 0.25 eV has been added to $E_{n,pyra}^{emis}$, which is a more significant change. These modifications have the effect of reducing the vacancy diffusion anisotropy ratio and increasing the stability of the pyramids that will hinder their vacancy emission.

Table 4: Comparison between the reference and optimized parametrizations.

Parametrization	Reference	Optimized
$E_{v,\parallel}^{m}$ (eV)	0.66	0.64
$E_{n,pyra}^{emis}$ (eV)	From 1.4 to 1.95 eV (depends on size see SM)	+0.25 eV
Simulation conditions		
T (K)	600	
Flux (dpa.s^{-1})	1×10^{-6}	
PKA energy (keV)	50	
Domain size (nm^3)	100×100×100	

Figure 10 shows the average diameter, the density of objects, and the density of point defects as a function of irradiation dose obtained by OKMC, as well as the experimental data used for the adjustment.

It can be seen in Figure 10a) that the three variants of interstitial loops (<a1>, <a2> and <a3>) generally have an equivalent mean size evolution with dose. There is, however, a small difference for variants <a2> and <a3> who have slightly larger sizes, an effect that is probably due to the lack of statistics (reduced defect number) and deserves further investigation in the future. The size evolution of these objects can be divided into 3 distinct stages (i) to (iii): (i)

between 0 and 0.5 dpa, there is a rapid growth of loops reaching an average diameter of about 2.4 nm; (ii) between 0.5 and 3 dpa, the loops no longer grow significantly (stationary stage); (iii) between 3 and 8 dpa, the growth is linear.

A different behavior is observed for the pyramids, their average size evolves in two distinct stages. The first is similar to the one of <a> interstitial loops with rapid growth reaching sizes of the order of 3 nm. The second stage corresponds to a linear increase (no stagnation).

As for <c> loops, they are quickly formed, but that they have a relatively slow evolution. The size of these objects remains rather constant, which may be due to vacancy diffusion anisotropy. Since the <c> loops are located in the basal plane, they are less likely to intercept the vacancies than in the isotropic case.

Although the <a> interstitial loops have an accelerated growth stage, we observe on Figure 10b) that their density is globally stationary from 0.5 dpa to 8 dpa and that the three family types have an equivalent density. There is a rapid increase in pyramid density from a dose of 3 dpa, the same dose for which <a> loop growth acceleration is observed. The <c> loop density is relatively low and also seems to increase for the same threshold of 3 dpa.

When comparing our results with those of the literature, it clearly appears (see for instance the TEM images of Jostsons et al [25]) that the size of the <a>interstitial loops is underestimated while their density number is overestimated [2]. Such a discrepancy can directly be ascribed to the immobility of interstitial clusters that we assumed in the model for sake of simplicity whereas they are known to be mobile [26]. The comparison performed however in terms of

point defect densities (estimated from the measured loops mean diameter and density assuming circular loops) shows a very good agreement, as shown in Figure 10c.

Figure 11 shows the macroscopic deformation obtained with the optimized parameterization. The trends obtained by OKMC are in very good agreement with the results of Carpenter et al [27], in particular the 3 growth stages are clearly reproduced. A slightly higher value of deformation in <a> directions is also obtained. It is important to mention that as shown in the Figure SM7 (Supplementary Material) the elongation in the basal plane is due to the <a> interstitial loops while the contraction along <c> is mainly due to the growth of the <c> vacancy loops.

Figure 12 shows the evolution of microstructures at different irradiation doses: the 1 dpa microstructure, typical of stage II, is rather homogeneous and a high density of <a> loops and pyramids is detected. There are also some small <c> loops. The 3dpa microstructure corresponds to the end of the stationary stage, we see the projection of layers of <a>interstitial loops parallel to the basal plane. The number of loops <c> is also higher than at 1 dpa.

During stage III (3 to 8 dpa), the acceleration of growth is associated with the formation of a layer of <a> interstitial loops. Also, some <c> loops have larger sizes than in the 3 dpa microstructure. Figure 12 shows an acceleration of the density of pyramids from 3 dpa, which has the effect of trapping the vacancies and allowing the acceleration of growth of interstitial objects. The microstructure at 8 dpa clearly shows an increase in the size of the interstitial loops. There is also distinctly an increase in the size and density of the <c>loops as well as an increase in the density of the pyramids. In Figure 11 and in the insert of Figure 12 it can be

seen that the acceleration of growth (the change in the growth slope) is rather due to the deformation induced by <a> loops than by <c> ones.

Discussion

The results of the reference and optimized parameterizations clearly show a phase of acceleration of macroscopic growth which is generated by the vacancy anisotropic diffusion. Indeed, when this latter is supposed isotropic, the growth rate is almost constant (Figure 7a). The microstructure analysis shows that in both cases, this acceleration growth is associated with the formation of interstitial <a> loops in sheets parallel to the basal plane, an arrangement that have been frequently reported in the literature but seldom explained. Two recent experimental works [4] [3] confirmed the strong correlation between the irradiation growth breakaway and this particular microstructural arrangement. In [4] it is shown that limited banding of <a> loops along basal traces is observed for irradiated low-Sn ZIRLO which is an alloy known for its strong resistance to radiation growth whereas in [3], it is stated that " … the proton-irradiated material demonstrates that the alignment of a-loops may be responsible for the nucleation of c-loops..". Therefore our simulations are totally in line with the most recent experimental observations.

An analytical model clearly shows that in this type of configuration, the absorption of self-interstitials by interstitial loops is optimal. During the growth acceleration stage, the excess remaining vacancies are absorbed by vacancy objects, but their evolution is not the same in the reference and optimized parameterizations:

- In the case where the stability of the pyramids is lower (reference parameterization), one single <c>loop increases significantly (Figure 5). Since the pyramids have a

higher emission capacity, there is a higher vacancy content in the system, which allows<c>loops to grow.

- When increasing the stability of the pyramids (optimized parameterization), acceleration occurs with an increase of pyramid densities (Figure 10).

Our simulations suggest that the incubation time to reach the growth acceleration stage is the time required for the interstitial loops to adopt their optimal configuration in layers parallel to the basal plane. As soon as this configuration is reached, the absorption of interstitials is maximal, which allows the growth of vacancy defects such as SFP and <c> loops. Since the work of Holt et al [28], it is admitted that there is a strong correlation between growth breakaway and the appearance of <c> component loops. Our work supports that there is also a correlation between the growth breakaway and the formation of band structures of <a> dislocation loops parallel to basal planes in agreement with recent experimental observations [3] [4].

This specific alignment of <a> loops in sheets parallel to the basal plane has often been experimentally observed [29, 25, 28, 1, 4, 3].The alignment of the interstitial loops in the basal plane obtained in our simulations clearly resembles the observations of these authors, and our paper proposes an explanation to this microstructural feature, in accordance with up-to-date diffusion data on point defects in zirconium. Based on the results of DFT modeling, the mobility of the vacancy is more anisotropic than that of the self-interstitial, and easier in the basal plane than perpendicular to it, which is the exact opposite of the hypothesis at the origin of the DAD model described in the literature [6] [22].

It is clear that the results presented in this work although particularly close to the experimental facts from a qualitative point of view, exhibit nevertheless some differences with those from a quantitative point of view. It is the case in particular

i- as far as the size of the <a> dislocation loops , of the order of 10 nm at some dpa for the optimized parametrization compared to roughly 100 nm from experiments shown in [25] .

ii- concerning the distance between the layers of <a> dislocation loops which is limited by construction to the size of the simulation cell i.e. 100 nm in the simulations presented here and are of the order of 400 nm in [25] .

iii- concerning the introduction of <a> vacancy dislocation loops, since their presence in the simulation at high density (simulations with p=0.5 and p=1) leads to a macroscopic growth and microstructure evolution that strongly deviates from experiments.

Point (i) can be unambiguously attributed to the lack of mobility of small interstitial clusters. In our work a di-interstitial is immobile and potentially a critical nucleus for an interstitial <a> loop formation. Assuming mobility of point defect clusters as observed by molecular dynamics in [26] should clearly induce coalescence of such small interstitial clusters, and therefore reduce the density of <a> dislocation loops while increasing their size. To include the mobility of small interstitial clusters in our model is possible at the cost of an increase in numerical complexity, a work that will be carried out in the near future.

Point (ii) can be probably related to the Vacancy Diffusional Anisotropy Ratio (VDAR). As presented here, no formation of layers of <a> loops is observed if isotropic diffusion is imposed for vacancies. Furthermore, the analytic model developed here shows that

preferential absorption of interstitials by rows or layers of loops parallel to the basal plane is favored when a VDAR > 1 is supposed.

Therefore a minimum value for VDAR >1 seems to be necessary to observe the formation of aligned layers of <a> interstitial loops parallel with the trace of the basal plane (0001). However, we can anticipate that a too strong value of VDAR should hinder the growth of the <c> vacancy loops and therefore inhibit their development. Our work therefore suggests that there exists a narrow window for VDAR , probably in the range 2-8 were two phenomena intricately related to irradiation growth can take place simultaneously : growth of <c> vacancy loops and formation of layers of <a> loops parallel to the basal plane.

As previously mentioned (iii) is probably due to the overestimation of the eigenstrain associated to <a> vacancy loops. According to our atomic scale modeling, <a> vacancy loops have a habit plane close to $\{1\,1\,\bar{2}\,0\}$ while experiments indicate a habit plane close to $\{1\,0\,\bar{1}\,0\}$. As a result their eigenstrain in the basal plane is close to -1, its maximum value (see Supplementary Material section). In comparison, <a> interstitial loops have, in agreement with experiments, a habit plane close to $\{1\,0\,\bar{1}\,0\}$ which leads to an eigenstrain of 0.5 in the basal plane. Whatever the origin of discrepancy with experiments, further work is needed to understand the influence of <a> vacancy loops in the evolution of microstructure under irradiation.

Based on previous works [17] [16] we have supposed here that <c> loops are formed by transformation of stacking fault pyramids which have not yet been clearly experimentally observed. We believe however that the idea of <c> vacancy loops not necessarily produced by agglomeration of individual defects is appealing and allows to explain why small size loops have not been yet observed. On the same order of ideas, a recent work [23] suggest that <c>

loops are formed by the interaction of preexisting <a> vacancy loops and cascades. Note however that such a mechanism can hardly explain the nucleation of <c> loops under electron irradiation.

Finally, we have shown here that allowing to form <a> vacancy loops in a significant amount (transition probability p=0.5) leads to the development of a microstructure which do not induce irradiation growth as experimentally observed. Studying the influence of the amount of such <a> vacancy loops on the microstructure is delayed for future works.

Conclusions

Combining Object Kinetic Monte Carlo modeling parametrized using state-of-the art atomic scale calculations, experimental data when available and an analytic analysis, we conclude that a Vacancy Diffusional Anisotropy Ratio (VDAR) greater than 1 (vacancy diffusion faster parallel to basal planes than perpendicularly to them) is necessary to observe irradiation growth of high purity recrystallized zirconium alloys under irradiation accompanied by the formation of banding of <a> interstitial loops parallel to the basal planes . We have associated the acceleration of growth to the concomitant formation of <c> vacancy loops and layers of <a> interstitial loops parallel to the basal planes. Our work suggests that there exists a narrow window of VDAR for which such a growth can occur. The modeling suggests that the contribution of interstitial <a> loops aligned in sheets parallel to the basal plane is at least as important as the contribution of <c> loops.

Acknowledgements

This work is part of the EM2VM Joint laboratory Study and Modeling of the Microstructure for Ageing of Materials. Part of the work was funded by the project CRAYON P11LY from

EDF. Calculations have been performed on EDF R&D HPC resources and we also acknowledge PRACE for awarding us access to resource MARCONI-KNL at CINECA in Italy and Hazel Hen at HLRS in Germany (project MORPHO e Modeling Radiation damage:characterization

of elementary PHysical prOcesses e Grant No 2016153636).

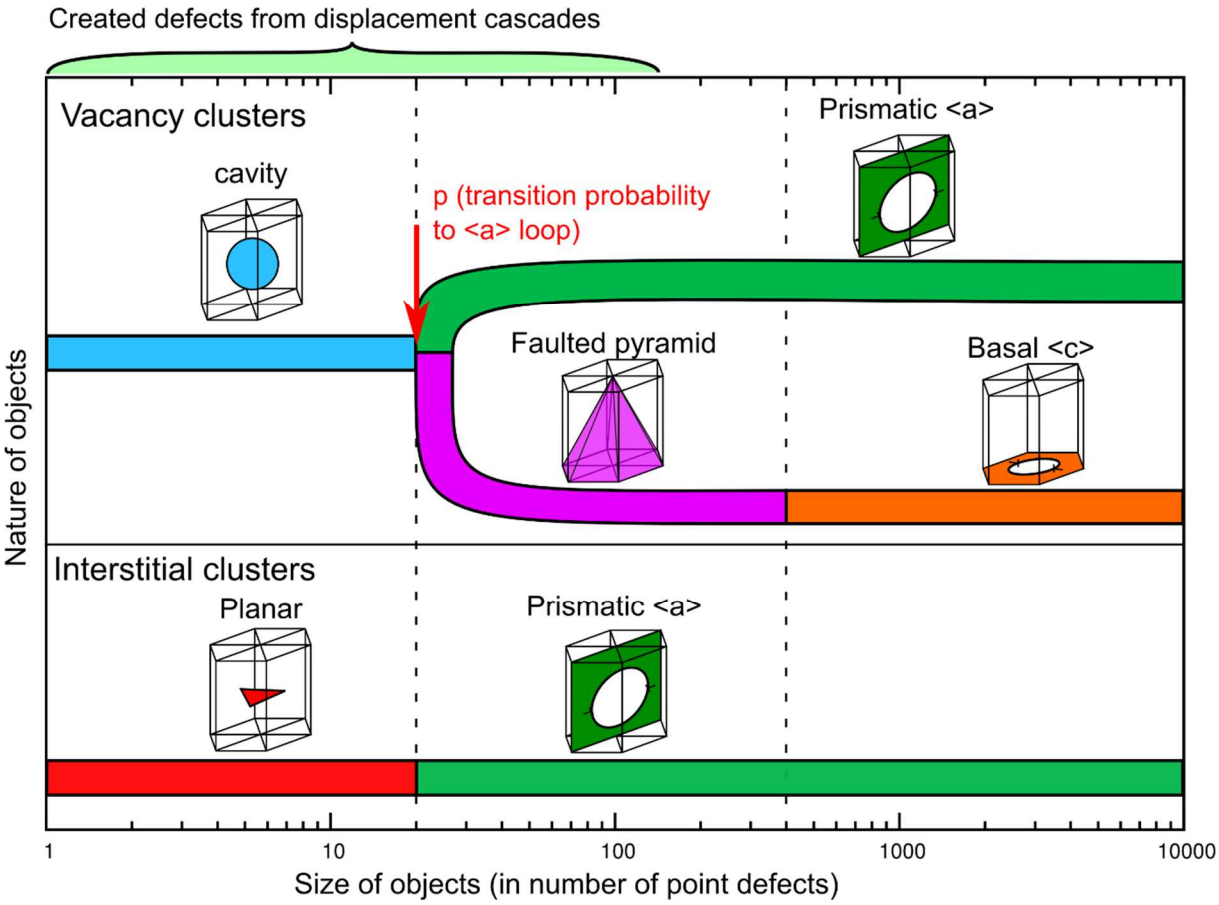

Figure1: schematics of the extended defects used during the OKMC simulations.

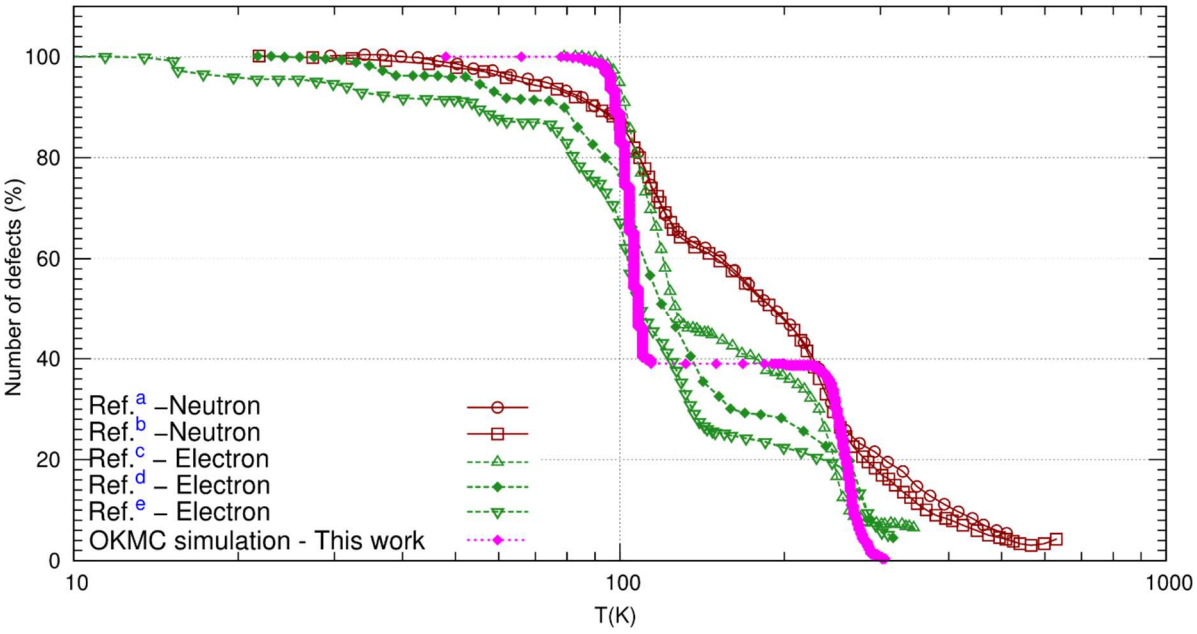

Figure2: OKMC simulation of post electron irradiation and isochronous annealing and comparison with experiments a) extracted from [30], b) extracted from [31], c) extracted from [32], d) extracted from [21], e) extracted from [33].

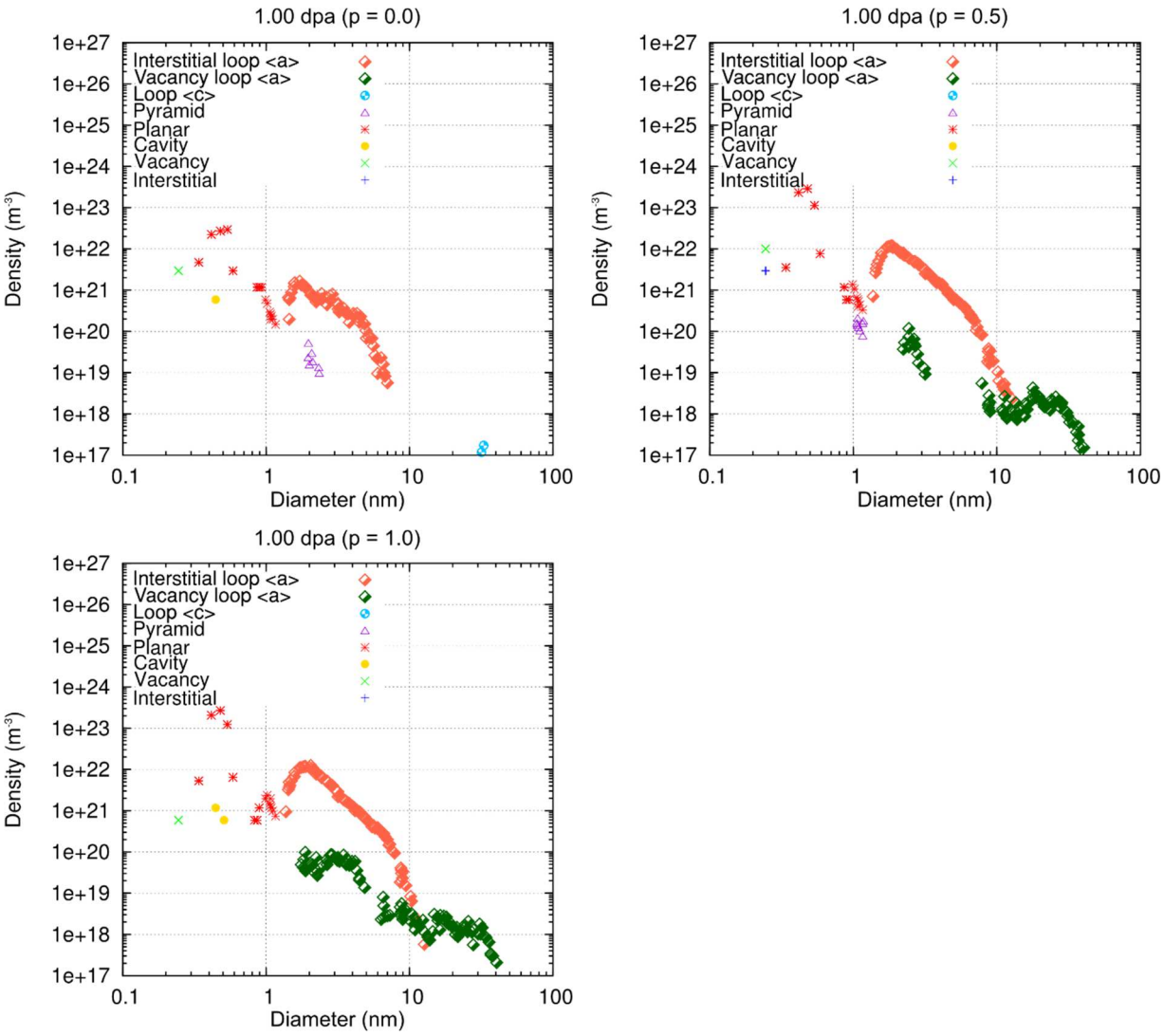

Figure 3: Defect density evolution (m^{-3}) as a function of their diameter (nm) at 1 dpa for different values of *p* (0, 0.5 and 1.0).

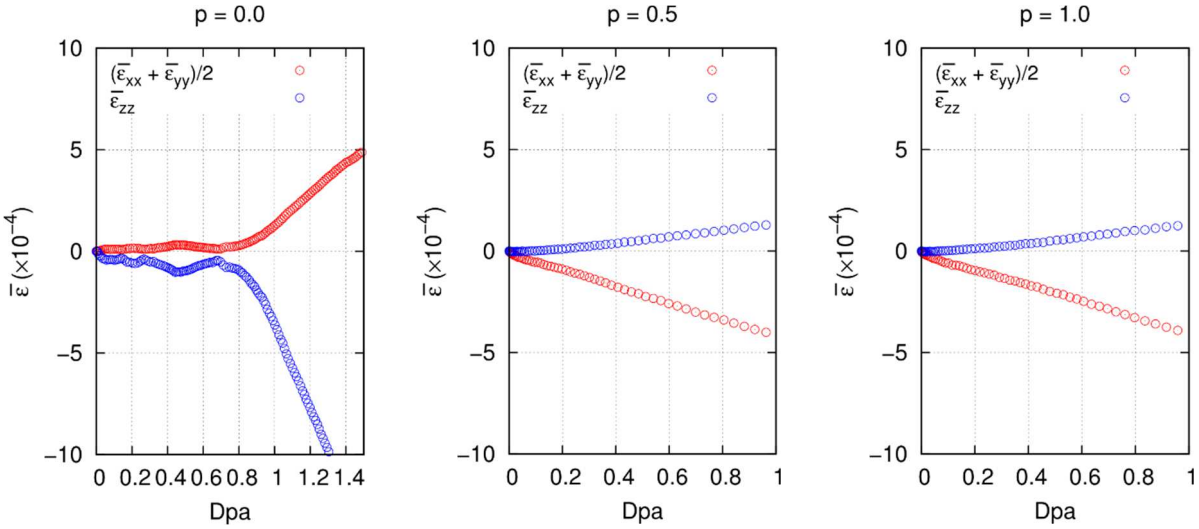

Figure 4: Macroscopic deformation of the crystal when anisotropic diffusion of the vacancy is taken into account for different values of p (0, 0.5 and 1).

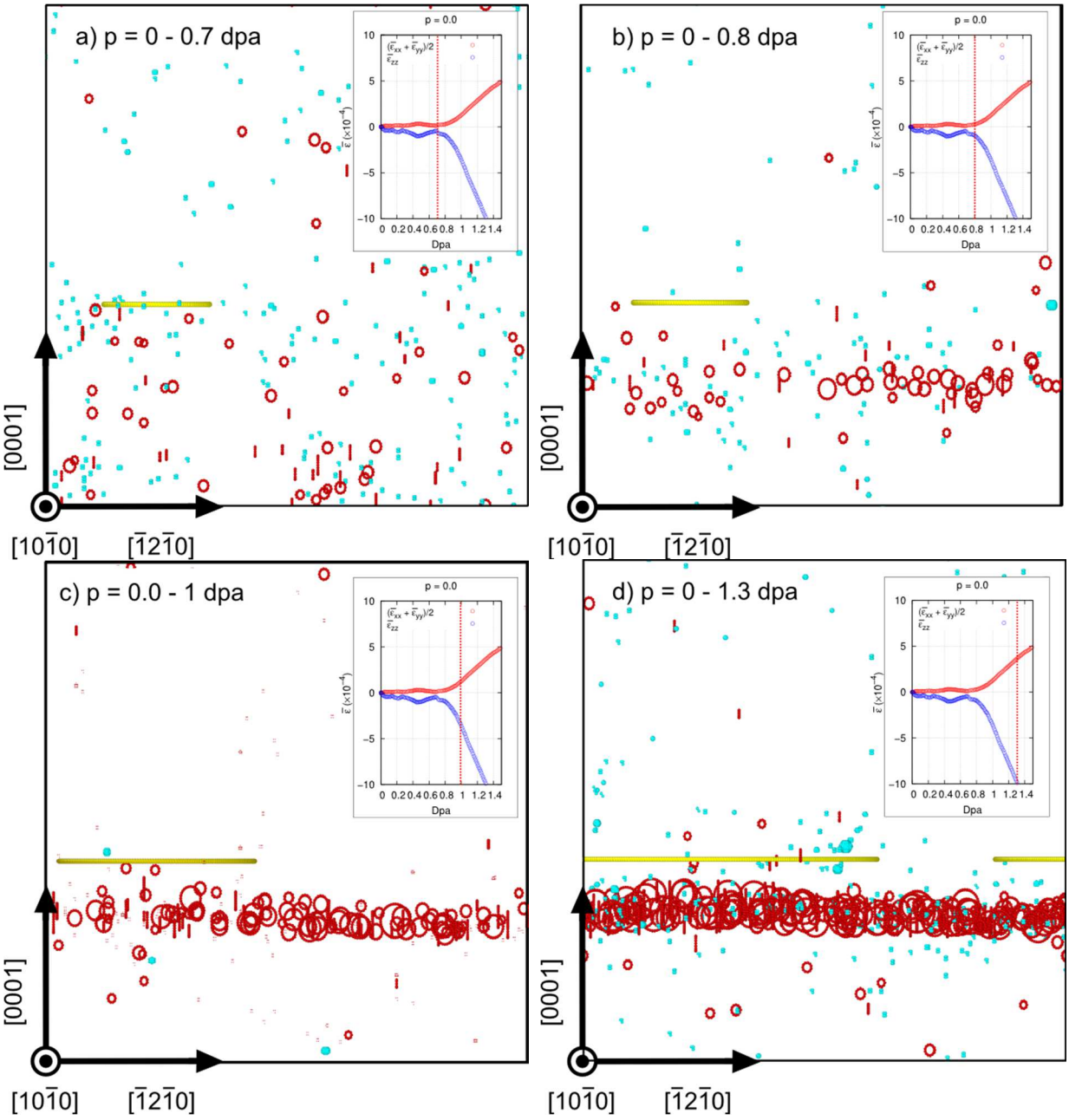

Figure 5: Microstructures obtained for p = 0 and different doses (0.7, 0.8, 1 et 1.3 dpa). <c> vacancy loops, <a> interstitial loops, pyramids (and cavities) are respectively represented in yellow, red and cyan. The onset gives the corresponding macroscopic deformation as a function of dose.

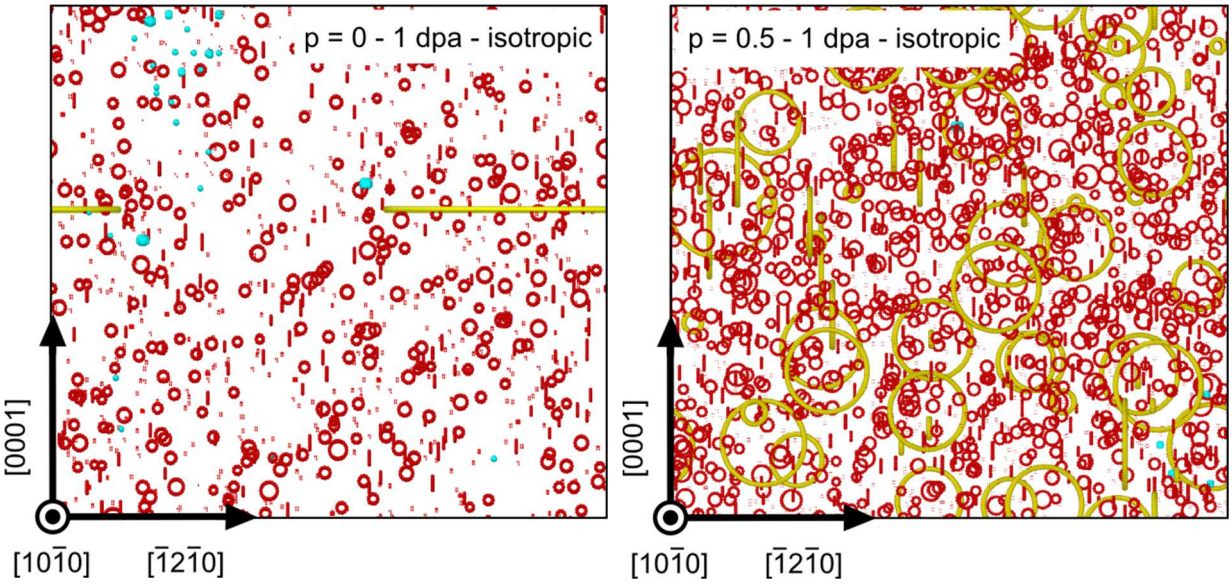

Figure 6: Microstructures obtained at 1dpa in the case of isotropic vacancy diffusion and two values $p = 0$ and $p = 0.5$: vacancy loops (<c> and <a>), <a> interstitial loops, pyramids (and cavities) are respectively represented in yellow, red and cyan.

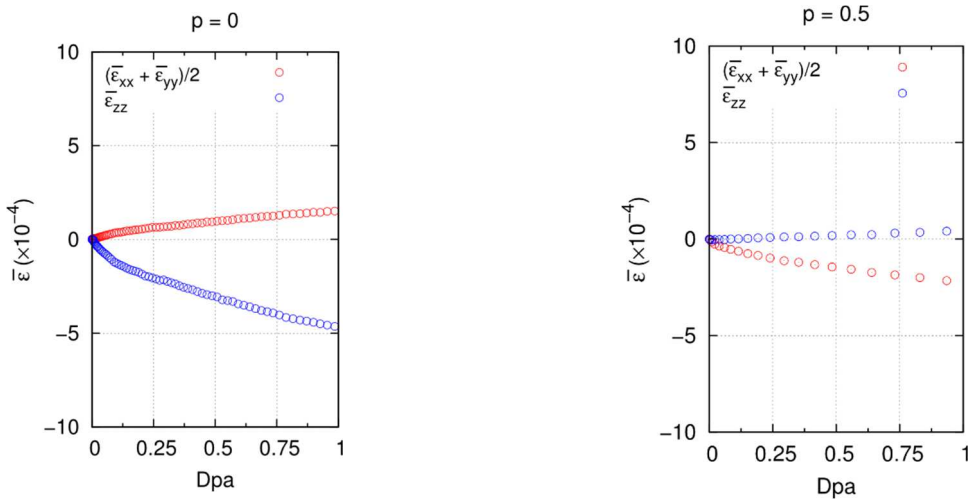

Figure 7: Free growth in the basal plane (red open circles) and along the c axis (blue open circles) in the case of isotropic vacancy diffusion for $p = 0$ (left) and $p = 0.5$ (right). The presence of <a> vacancy loops for p=0.5 leads to an anisotropic growth at odds with experiments (see text).

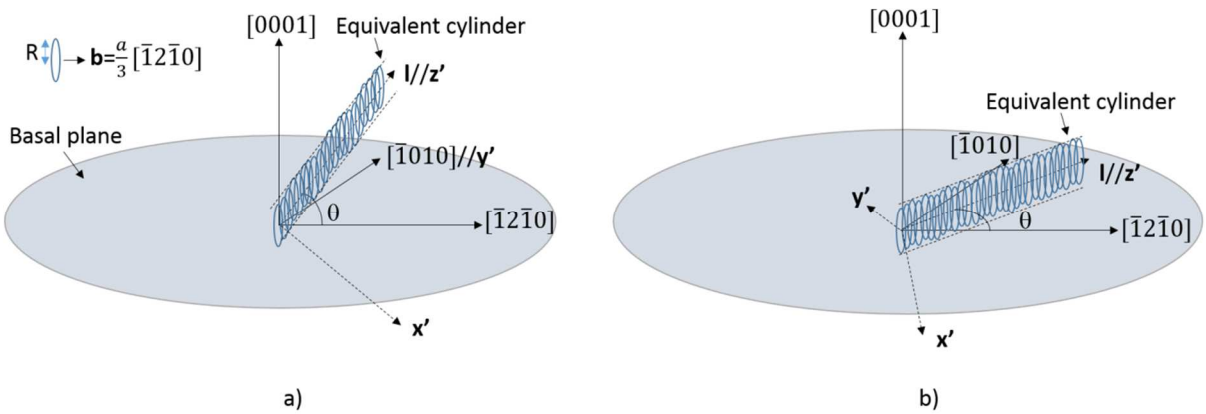

Figure 8: Stacking of prismatic loops of Burgers vector b = 1/3 $[1\ 1\ \bar{2}\ 0]$ and radius R along the **l** direction located in the a) prismatic and b) basal plane. Direction **l** is defined by the angle θ which is measured with respect to $[1\ 1\ \bar{2}\ 0]$ in both cases. (x',y',z') is an intermediate basis used to calculate the fluxes of vacancies and self-interstitials absorbed by the stacking of prismatic loops.

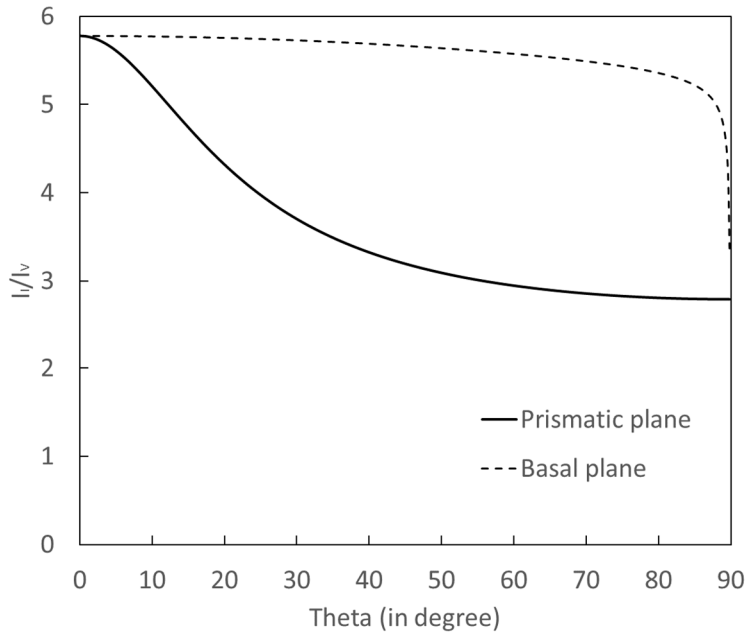

Figure 9:
Ratio between the flux of interstitials I_I and the flux of vacancies I_V absorbed by a cylinder equivalent to the stacking of prismatic loops as a function of its orientation θ defined in Figure 8 in the prismatic (solid line) or basal (dotted line) plane.

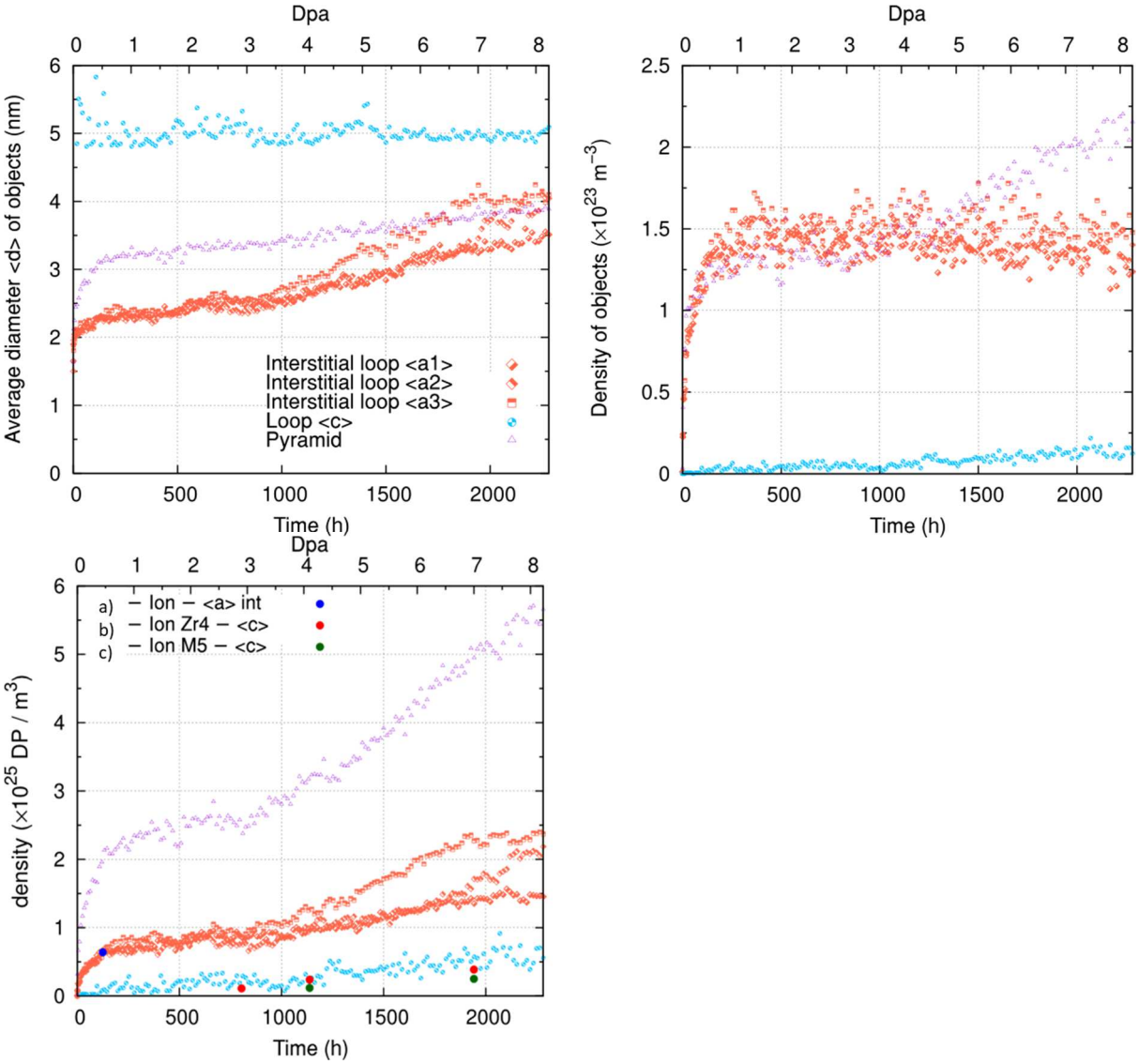

Figure 10: Average diameter, object and point defects densities as a function of the irradiation dose for the optimized parametrization. The point defects density is compared with experimental data a) extracted from [2], b) and c) extracted from [24]. They were estimated from the Transmission Electron Microscopy measured mean diameter and density of loops assuming circular loops.

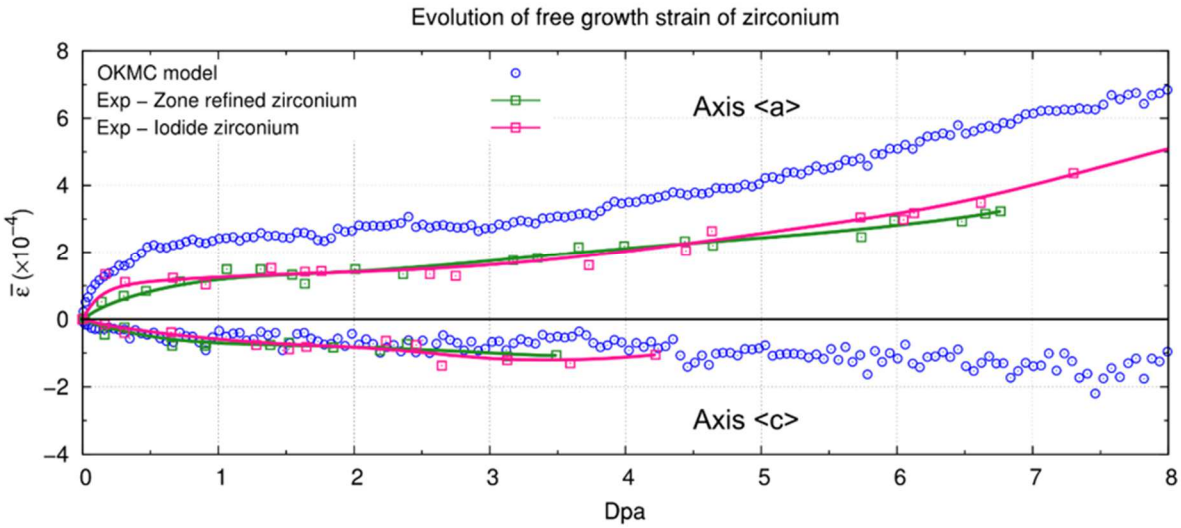

Figure 11: Macroscopic deformation obtained in the case of the optimized parameterization as a function of the irradiation dose. Comparison with experiments [27].

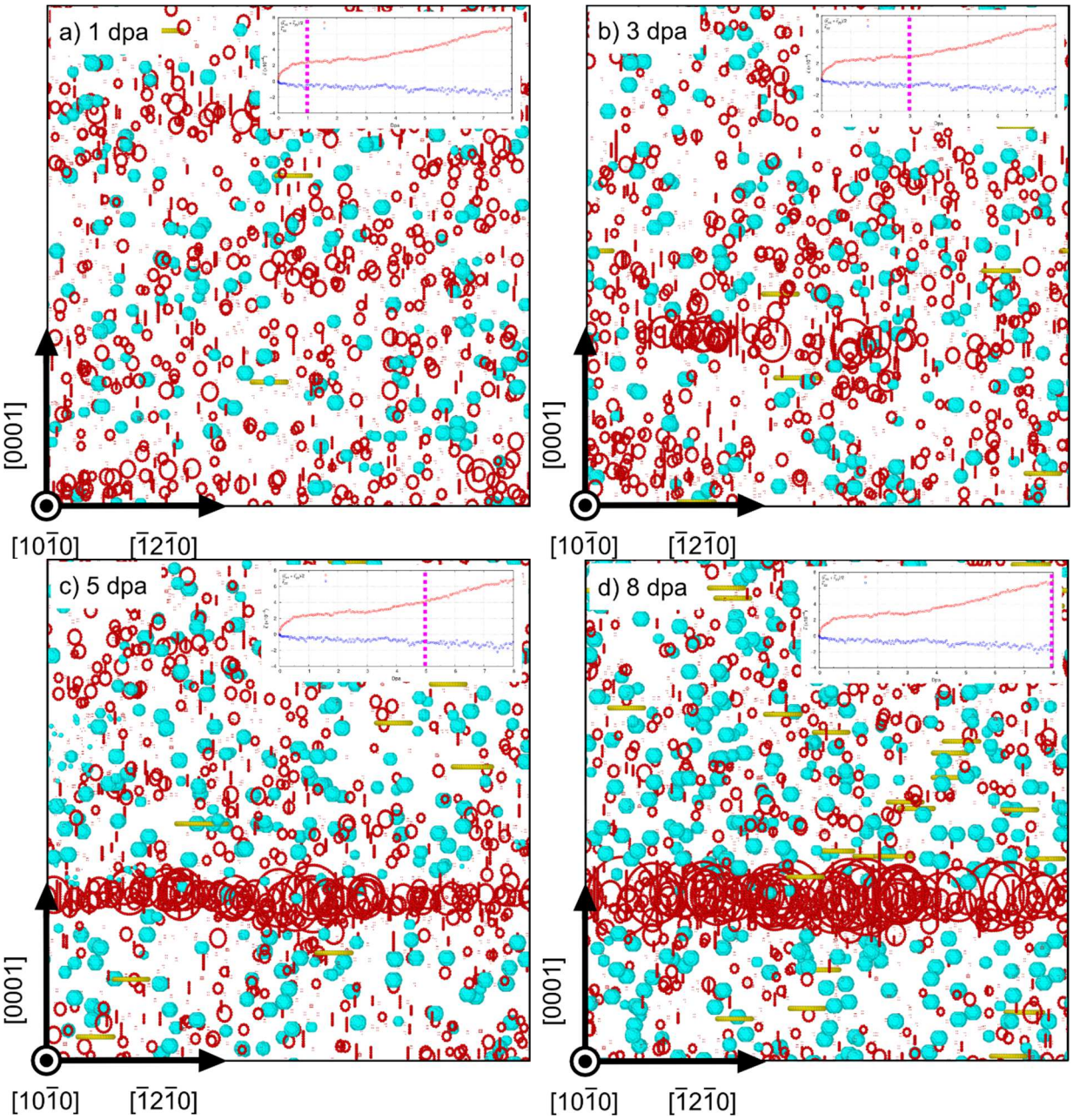

Figure 12: Macroscopic deformation obtained in the case of the optimized parameterization as a function of the irradiation dose. ‹c› vacancy loops, ‹a› interstitial loops, pyramids (and cavities) are respectively represented in yellow, red and cyan.

Bibliography

[1] M. Griffiths, «A review of microstructure evolution in zirconium alloys during irradiation,» *J. Nucl. Mater. ,* vol. 159, pp. 190-218, 1988.

[2] M. Gaumé, F. Onimus, L. Dupuy, O. Tissot, C. Bachelet et F. Mompiou, « Microstructure evolution of recrystallized Zircaloy-4 underchargedparticles irradiation,» *J. Nucl. Mater. ,* vol. 495 , p. 516–528, 2017.

[3] A. Harte, D. Jädernäs, M. Topping, P. Frankel, C. P. Race, J. Romero, L. Hallstadius, E. C. Darby et M. Preuss, «The effect of matrix chemistry on dislocation evolution in an irradiated Zr alloy,,» *Acta Materialia ,* vol. 130 , pp. 69-82, 2017.

[4] E. Francis, R. Prasath Babu, A. Harte, T. Martin, P. Frankel, D. Jädernäs, J. Romero, L. Hallstadius, P. Bagot et M. Preuss, «Effect of Nb and Fe on damage evolution in a Zr-alloy during proton and neutron irradiation,» *Acta Materialia ,* vol. 165, pp. 603-614 , 2019.

[5] F. Onimus et J.-L. Béchade, «Radiation Effects in Zirconium Alloys,» *Comprehensive Nuclear Materials,* vol. 4, pp. 1-31, 2012.

[6] C. Woo, «Theory of irradiation deformation in non-cubic metals,» *J. of Nucl. Mat.,* vol. 159, pp. 237-256, 1988.

[7] G. Samolyuk, A. Barashev, S. Golubov, Y. Osetsky et R. E. Stoller, «Analysis of the anisotropy of point defect diffusion in hcp Zr,» *Acta Materialia,* vol. 78, pp. 173-180, 2014.

[8] G. Vérité, Structure, stabilité et mobilité des défauts ponctuels dans le zirconium hexagonal compact : étude ab initio, Université Pierre et Marie Curie- Paris VI, 2007.

[9] P. Gasca, Zirconium – modélisation ab initio de la diffusion des défauts ponctuels, UNIVERSITE LILLE 1 – SCIENCES ET TECHNOLOGIES , 2010.

[10] J. Hood, H. Zou, D. Gupta and R. Schultz, "Alpha-Zr Self Diffusion Anisotropy," *Journal of Nuclear Materials,* vol. 223, pp. 122-125, 1995.

[11] R. Bullough, B. Eyre et K. Krishan, *Proc. R. Soc. ,* vol. A346, p. 81, 1975.

[12] A. Barashev, S. Golubov et R. Stoller, «Theoretical investigation of microstructure evolution and deformation,» *Journal of Nuclear Materials ,* vol. 461 , p. 85–94, 2015.

[13] C. Domain, C. Becquart et L. Malerba, *J. Nucl. Mater,* vol. 335 , p. 121, 2004.

[14] Y. Osetsky, D. Bacon et N. D. Diego, «Anisotropy of point defect diffusion in alpha-zirconium,» *Metall. Mater. Trans. A,* vol. 33, p. 777–782, 2002.

[15] F. Christien et A. Barbu, «Effect of self-interstitial diffusion anisotropy in electron-irradiated zirconium: a cluster dynamics modeling,» *J. Nucl. Mater.,* vol. 346, p. 272–281, 2005.

[16] B. Christiaen, C. Domain, L. Thuinet, A. Ambard et A. Legris, «A new scenario for <c>vacancy loop formation in zirconium based on atomic-scale modeling,» *Acta Materialia,* pp. 93-106, 2019.

[17] B. Christiaen, Modélisation multi-échelle de la déformation d'alliages de zirconium sous irradiation, UNIVERSITÉ DES SCIENCES ET TECHNOLOGIES DE LILLE, 2018.

[18] R. Voskoboinikov, Y. Osetsky et D. Bacon, «Interactions with Materials and Atoms Identification and morphology of point defect clusters created in displacement cascades in α-zirconium,» *Nuclear Instruments and Methods in Physics Research Section B: Beam,* vol. Volume 242, pp. 530-533, 2006.

[19] G. Hood, H. Zou, R. Schultz, N. Matsuura, J. Roy et J. Jackman, «Self-and Hf diffusion in alpha-Zr ans in Dilute, Fe-Free, Zr(Ti) and Zr (Nb) Alloys,» *Defect and Diffusion Forum ,* Vols. %1 sur %2143-147, pp. 49-54, 1997.

[20] F. Christien et A. Barbu, «Cluster Dynamics modelling of irradiation growth of zirconium single crystals,» *J. Nucl. Mater.,* p. 153–161, 2009 .

[21] F. Dworschak, C. Dimitrov et O. Dimitrov, « Interaction of self-interstitials with oxygen atoms in electron-irradiated zirconium,» *J. Nucl. Mater.,* vol. 82 , p. 148–154, 1979.

[22] C. Woo et U. Gösele, «Dislocation bias in an anisotropic diffusive medium and irradiation growth,» *J. Nucl. Mater.,* vol. 119, pp. 219-228, 1983 .

[23] C. Dai, P. Saidi, M. Topping, L. Béland, Z. Yao et M. Daymond, «A mechanism for basal vacancy loop formation in zirconium,» *Scripta Materialia,* vol. 172, pp. 72-76, 2019.

[24] N. Gharbi, Contribution to the understanding of zirconium alloydeformationunder irradiation at high doses, Thèse, Université de La Rochelle, 2015.

[25] A. Jostsons, P. Kelly et R. Blake, «The nature of dislocation loops in neutron irradiated zirconium,» *J. Nucl. Mater,* vol. 66, p. 236–256, 1977.

[26] N. d. Diego, Y. Osetsky et D. Bacon, «Mobility of Interstitial Clusters in Alpha-Zirconium,» *Matallurgical and Materials Transactions A,* vol. 33A, pp. 783-789, 2002.

[27] G. Carpenter, R. Zee et A. Rogerson, «Irradiation growth of zirconium single crystals: A review,» *J. Nucl. Mater.,* vol. 159, p. 86–100, 1988.

[28] R. Holt et R. Gilbert, «< c> Component dislocations in annealed Zircaloy irradiated at about 570 K,» *Journal of Nuclear Materials. ,* vol. 137 , p. 185–189, 1986.

[29] P. Kelly, R. Blake et A. Jostsons, «An interpretation of corduroy contrast in neutron irradiated zirconium,» *J. Nucl. Mater.,* vol. 59 , p. 307–315, 1976.

[30] M. Anand, W. Mansel, G. Wallner et W. Weck, « Damage rate measurements at 4.6 K and recovery studies in zirconium and zirconium-tin alloys,» *Radiat. Eff. ,* vol. 89, p. 179–187, 1985.

[31] P. Vialaret, F. Moreau, A. Bessis, C. Dimitrov et O. Dimitrov, «Etude des défauts ponctuels dans le zirconium irradie par les neutrons a 24 K,» *J. Nucl. Mater. ,* vol. 55 , p. 83–95, 1975.

[32] В. Борисенко, Ю. Петрусенко, Д. Баранков et П. Вьюгов, «Изохронныйотжигсплавов Zr-Sc и Zr-Y, облученных 2 МэВэлектронами,,» *ВопросыАтомнойНауки И Техники.,* 2008.

[33] H. Neely, «Damage rate and recoverymeasurements on zirconium afterelectron irradiation at lowtemperatures,» *Radiat. Eff.,* vol. 3 , p. 189–201, 1970 .

[34] F. Nabarro, «CXXII. The synthesis of elastic dislocation fields.,» *The London, Edinburgh, and Dublin Philosophical Magazine and Journal of Science,* vol. 42, pp. 1224-1231, 1951.

[35] C. S. Becquart, K. M. Decker, C. Domain, J. Ruste, Y. Souffez, J. Turbatte et J. V. Duysen, «Massively parallel molecular dynamics simulations with EAM potentials.,» *Radiation Effects and Defects in Solids ,* vol. 142, pp. 9-21, 1997.

[36] .. Mendelev et G. Ackland, «Development of an interatomic potential for the simulation of phase transformations in zirconium,» *Philos. Mag. Lett. ,* vol. 87, pp. 349-359, 2007.

[37] M. Norgett, M. Robinson et I.M.Torrens, «A proposed method of calculating displacement dose rates,» *Nuclear Engineering and Design,* vol. 33, pp. 50-54, 1975.

Combine atomic scale modeling with analytical models

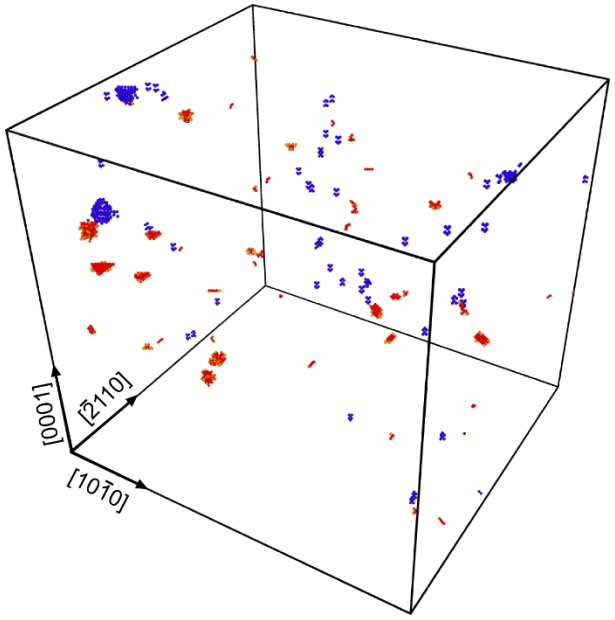

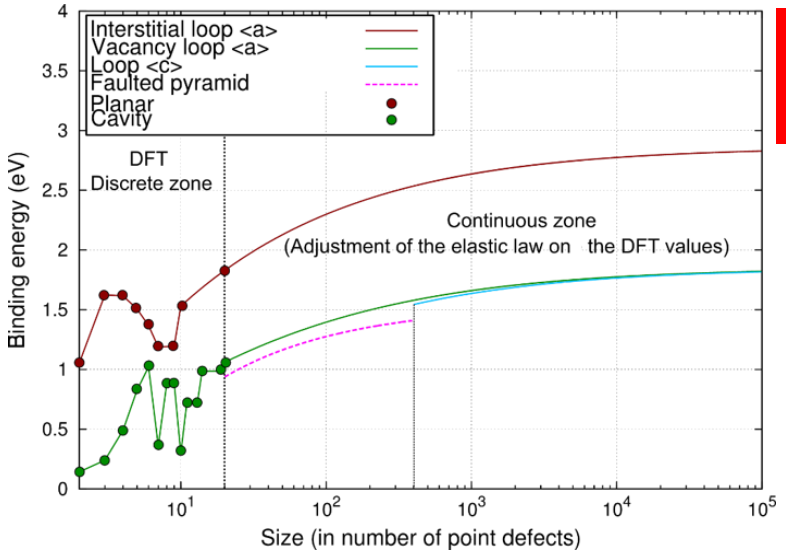

Feed an Object Kinetic Monte Carlo model

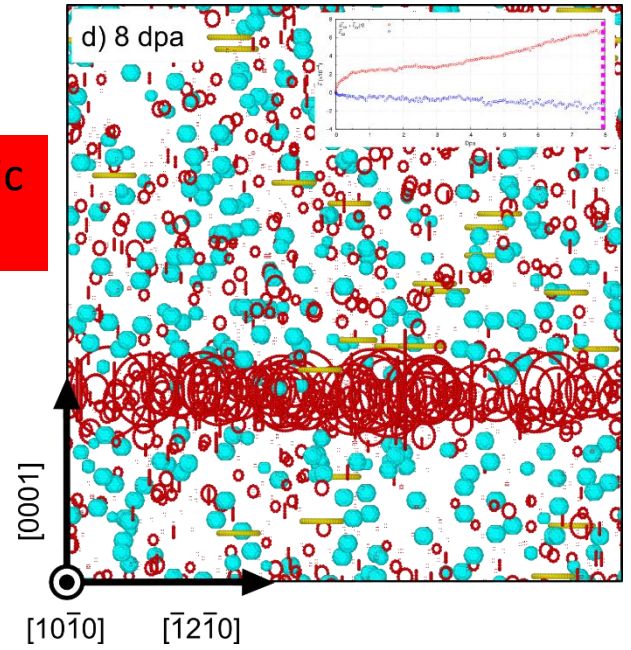

Microstructure evolution

Cascades: Molecular Dynamics

Extrapolate atomic scale data through analytical models

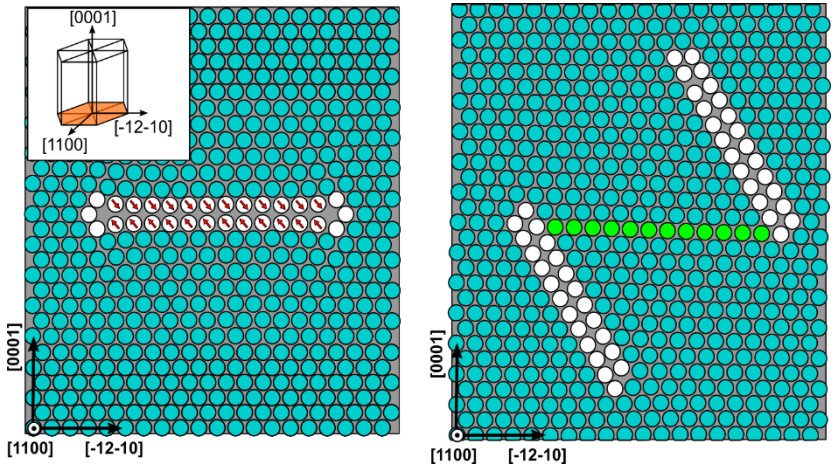

Extended defects: DFT and empirical potentials
Energy minimization

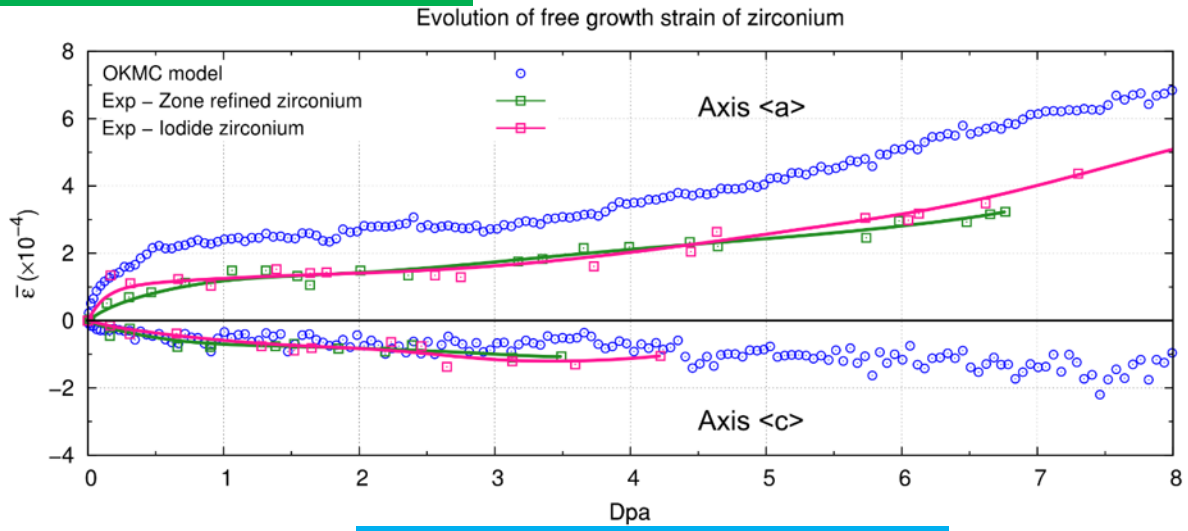

Explain macroscopic growth